Composite Structures 299 (2022) 116097

Contents lists available at ScienceDirect

Composite Structures

journal homepage: www.elsevier.com/locate/compstruct

Mechanical behavior of woven CMCs under non-uniform stress and strain fields

Zheng-Mao Yang [a,d,*], Jing-Yu Sun [a], Jun-Jie Yang [b], Tian-Wei Liu [a], Hui Liu [c]

[a] Institute of Mechanics, Chinese Academy of Sciences, Beijing, China
[b] Institute for Aero engine, Tsinghua University, Beijing, China
[c] Beijing Institute of Astronautical Systems Engineering, China Academy of Launch Vehicle Technology, Beijing, China
[d] School of Engineering Science, University of Chinese Academy of Sciences, Beijing, China

ARTICLE INFO

Keywords:
Ceramic-matrix composites (CMCs)
Non-uniform strain
Finite element analysis
Mechanical properties
Weave architecture

ABSTRACT

Woven ceramic matrix composites (CMCs) hot-section components will sustain spatially non-uniform stress and temperature fields in service, and the mechanical response in CMCs under inhomogeneous stress and strain fields remains indistinct. This study focuses on one noteworthy aspect of this issue: the effects of weave architecture on the mechanical response of CMCs under off-axis and thermomechanical loading. To this end, the stress and strain evolution of wavy tows in CMCs are investigated by establishing a meso-scale finite element model, which reflects the real weave architecture. Besides, the model is verified by comparing the predicted results with the experimental results of a representative woven CMC. The strain and stress concentrations appear at the location of tow cross-overs because of the bending and straightening of tows, resulting in the woven composites strength may be inferior to that of laminate composites. Although the scope of this work is limited to one type of weaving, it is expected that the modeling method can be useful in examining other types of weaving.

1. Introduction

Woven ceramic matrix composites (CMCs) are the core strategic materials for thermal protection systems of hypersonic vehicles (Ma>5) and hot-section components of advanced aero-engines [1–4], with higher out-of-plane stiffness, strength, and toughness properties compared with unidirectional composites. During the service process, CMCs components will undergo high temperatures above 1200 °C, complex loading and large temperature gradient thermal shocks, with the addition of braided structure and porosity in CMCs, non-uniform stress and strain fields will arise in wavy tows of CMCs [5,6]. Compared with laminated composites, the initial failure may arise earlier in the most seriously strained areas of woven composites due to the spatially non-uniform strains [7,8]. Moreover, the defects, such as pores and sintering cracks [9,10], in the matrix of CMCs will exacerbate the non-uniform strains. It is a challenging issue to accurately describe and predict the mechanical behavior of fiber-reinforced CMCs under heterogeneous stress and temperature fields.

There is a great challenge to extend the traditional mechanical approaches and frameworks used for laminated composites to the analysis of woven CMCs, due to the complexity of material composition and microstructure of woven CMCs, such as heterogeneous matrix and wavy tows [11]. Therefore, researchers have been devoted to applying the computational method to predict the deformation and distribution of woven composites, and further progress has been made [12]. Cox et al. [13] investigated the effects of stochastically varying microstructure on the damage evolution of continuous-fiber composites by establishing a finite element (FE) model, it should be mentioned that the virtual specimen generator was used to obtain the idealized FE model of weave architecture. Zhang et al. [14] developed an FE-based model for an 8 harness satin woven (8HSW) CMC, and the stress–strain relationship, as well as fracture behavior, can be predicted using the approach, considering the strain-induced damage. Shojaei et al. [15]investigated the microscale damage mechanisms in CMCs and developed a continuum damage mechanics (CDM) model to study matrix/interphase fracture and fiber sliding. As for the multiscale modeling of composites, Leonetti [16] proposed a multiscale method to investigate the masonry structures considered periodic composites, which can be extended to woven composites with periodic architectures. Colatosti [17] applied micropolar modeling to a composite consisting of rectangular rigid blocks and elastic interfaces, and the non-local theory was used to take into account scale effects. To capture the influence of through-thickness constraint on the stress and strain

* Corresponding author.
E-mail address: zmyang@imech.ac.cn (Z.-M. Yang).

https://doi.org/10.1016/j.compstruct.2022.116097
Received 18 October 2021; Received in revised form 12 May 2022; Accepted 8 August 2022
Available online 12 August 2022

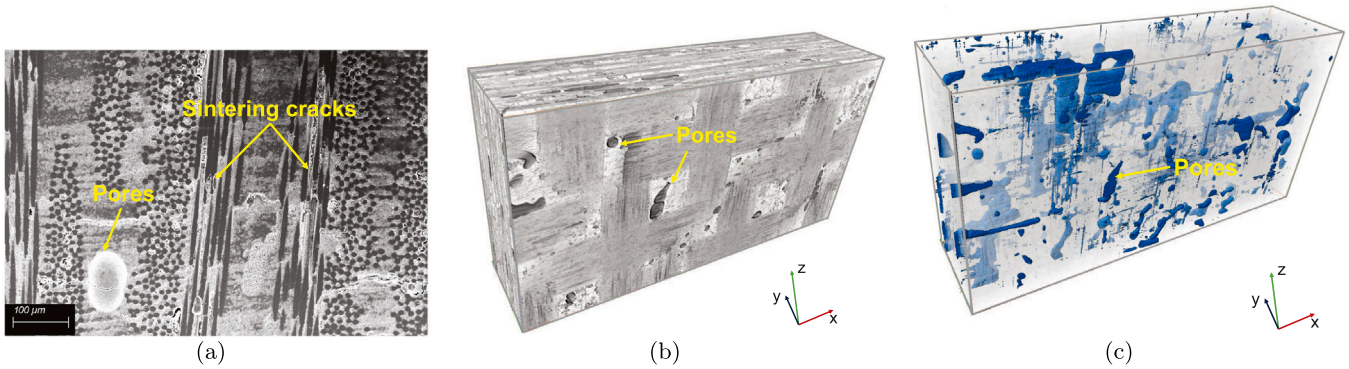

Fig. 1. Microstructural analysis of the composite. (a) Cross-sectional surface of a $[0/90]_S$ lay-up, reveal extensive sintering shrinkage microcracking perpendicular to the plies and some remnant porosity in the matrix; (b) Volume reconstruction of the microstructure by high resolution X-ray computer tomography data; and (c) Representation of the hierarchical pores present in the composite, the blue color represents pores.

distribution, Rossol et al. [1] developed a series of meso-scale FE models for an 8HSW SiC/SiCN composite, including one-ply, two-ply, four-ply, two-ply infinite model, and the effects of weave architecture were also studied. However, most of the research focus on the stress–strain response of the woven composites under on-axis tensile loading, the CMCs components often suffer off-axis or 2-D loading in actual situations. Therefore, it is of importance to capture the material response and the effects weave architecture of CMCs under off-axis loading.

Significantly less attention has been devoted to 2-D loadings, wherein the stress is not aligned with the tow axes [18–21]. Predicting deformation and fracture in these loadings requires that the off-axis response of the composite, as manifested in its 45° tensile behavior, be accurately captured. Lu et al. [22] investigated the damage behavior of on-axis and off-axis tension for 2.5D woven composites, by means of a multi-scale progressive damage model, and the deformation mechanisms and tensile strength were obtained. Zhang et al. [23] found the effects of the off-axis angles on the material behaviors, damage change, as well as failure mechanisms, and they founded that the main failure modes for off-axis samples are debonding and pull-out breakage. Yang et al. [24] utilized the digital image correlation to capture the strain distribution of orthotropic woven carbon-epoxy composites when they are under off-axis tensile loading, the load-bearing and failure mechanisms were also observed. Kesba et al. [25] established a modified shear-lag model to investigate the influence of crack density on different off-axis angles of composite layers. Yang et al. [26] developed strain partitioning and damage decoupling methods in studying the behavior of CMCs under macroscopic plane stress. From the literature survey, most investigation concentrate on the macroscopic failure mechanism or deformation response for woven composites under off-axis loading, the quantitative knowledge of the role that the weave architecture plays during the off-axis loading remains imperfect.

In addition to the off-axis response of CMCs, the thermomechanical loading is another factor causing the non-uniform stress and strain fields. Kastritseas et al. [27,28] investigated the onset of multiple matrix cracking in unidirectional CMCs under thermal shocks, and a semi-empirical formula was established to obtain the critical temperature gradient. Mei et al. [29] compared the mechanical response of 2D and 3D C/SiCs suffering mechanical fatigue and thermal cycling, and the residual strengths and microstructural characterization were used to assess the damage. Han et al. [30] investigated the effects of thermal residual stress on the strength of composites by establishing a microscopic computational model. Yang et al. [31] developed a continuum damage model for 2D woven CMCs under thermal shocks, and the microstructure evolution, as well as thermomechanical damage, were also represented [32]. Despite that many researchers have been devoted to the macroscopic qualitative characterization of CMCs under thermal shocks [33–35], the influence of non-uniform stress and strain on mechanical response under thermal shocks still need attention.

The principal objectives of the present work are: (i) provides insights into the mechanical response of woven CMCs under non-uniform stress and strain fields; and, (ii) probes the effects of off-axis loading and thermo-mechanical loading on fiber stress and strain distributions. In view of this, a meso-scale FE model of woven CMCs is established considering the effects of porosity. To assess the proposed FE model and material property, the macroscopic material responses of the finite element model will be compared with the experimental results under off-axis tensile and thermo-mechanical loadings. The stress and strain distributions, the role of matrix properties considering the porosity, and the potential fracture initiation will be investigated by the FE results of woven CMCs.

2. Materials and experiments

2.1. Materials

To investigate the effects of the weave architecture for CMCs under non-uniform stress and strain fields, the 8HSW oxied/oxied-CMCs(ox/ox-CMCs) was chosen as the object of study, which consists of uncoated Nextel™ 610 (99% $\alpha - Al_2O_3$) fibers and $Al_2O_3 - SiO_2 - ZrO_2$ matrix, with the lay-up of $[0/90]_{2s}$. The volume fraction of the fiber phase is 44%, and the density is 4.0 g/cm^3. The density of the matrix is 4.2 g/cm^3, then the total material density is 2.71 g/cm^3. The finished composite panel is 2.8 mm in thickness.

It should be mentioned that there are hierarchical pores in the ox/ox-CMCs due to the manufacturing process, which can be demonstrated by micro-CT, as shown in Fig. 1. The pores in the materials can be taken into two populations: the first one can be observed in the matrix with a diameter of a few nanometers, so-called nanopores; the other one named micropores exists in both matrix and fibers, with a diameter of a few microns. The cause of the formation for hierarchical pores may be divided into two aspects: When the gas is trapped in the matrix during the material process, the pores will take shape [36]. Besides, during the fabrication process, the high-temperature gradient will cause thermal stress in the fiber and matrix, and the mismatch of the coefficient of thermal expansion (CTE) may lead to excessive microcracks. The hierarchical pores play an important role in the mechanical response, which has been discussed in the previous work [32,37].

2.2. Experiments

2.2.1. Cyclic thermal shocks

As CMCs are widely used in thermal protection systems, extreme temperature environments may cause the failure of the CMC components. It is significant to investigate the material response under thermomechanical loading. Cyclic thermal shock, as a typical thermo-mechanical loading in service and is easy to quantify [24], was chose

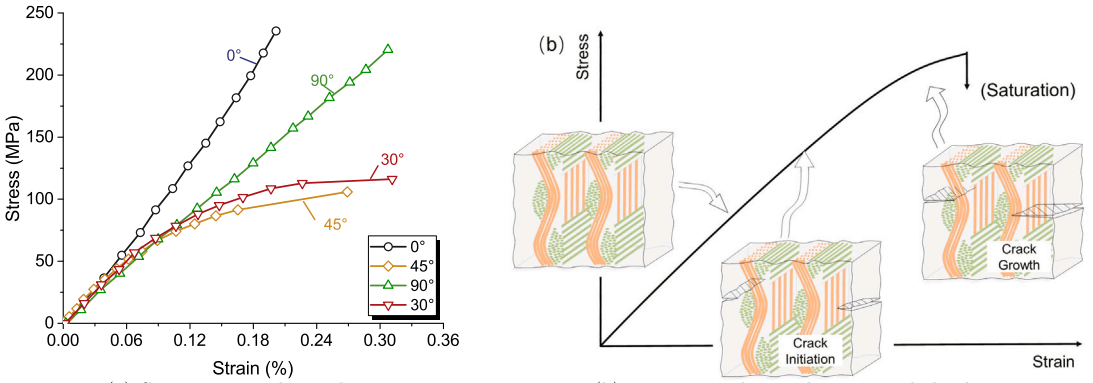

Fig. 2. (a) The stress–strain response with different off-axis angles of the ox/ox-CMCs; (b) Damage evolution during tensile loading, with the strain increases, cracks occur in the matrix and the material has permanent deformation, if the crack extends to the fiber bundles and lead to the failure of fibers, the material loses its carrying capacity.

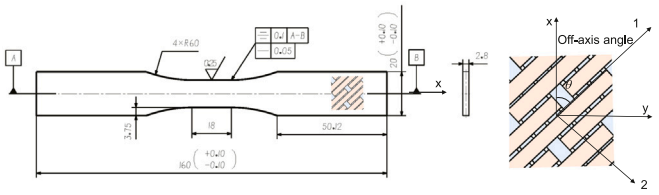

Fig. 3. Geometry of the uniaxial tension specimens and the off-axis angle.

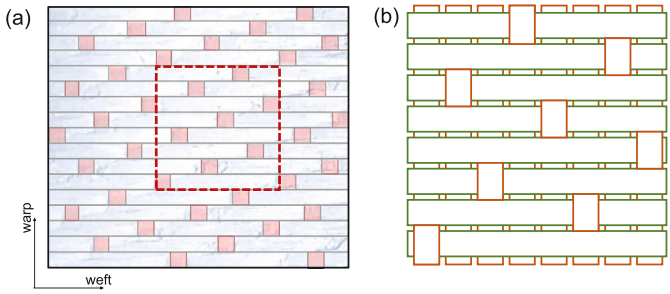

Fig. 4. (a) The real paths of weft and warp tows in CMCs were obtained by the SEM observation, which were used for the establishment of RUC; (b) The final weave architecture of the RUC, which contains eight weft tows and eight warp tows.

to study the effects of thermomechanical loading on the mechanical response in the present work.

The thermal shock experiments are conducted by heating the specimens to 1100 °C using the muffle furnace, and holding for 10 min to confirm the uniform temperature of the specimens, then putting the specimens into the water for cooling. Repeating the above process, the specimens can suffer cyclic thermal shocks. For the details of cyclic thermal shock tests can refer to the authors' previous work [37]. Then the thermal shocked specimens were performed on-axis tensile loading at room temperature.

2.2.2. Off-axis tension tests

Besides, to investigate the effects of off-axis loading, the off-axis tension tests were performed for the original CMC specimens, and 0°, 30°, 45°, 90° off-axis was chosen to discern the stress–strain relationship. The geometry of the different off-axis angle specimen is illustrated in Fig. 3, and the tension tests were performed on a MTS 809 servo-hydraulic test machine under displacement control, the displacement control speed is 10^{-4} mm/s. The dimensions of the specimen and test methods are referred to ASTM standards designated C1275-00.

2.3. The stress–strain response behavior

The stress–strain response with different off-axis angles for the ox/ox-CMCs were obtained, as shown in Fig. 2(a). In general, the stress–strain behaviors of different off-axis angles consists of three regions until it fails: (i) In the first region, the curves are nearly linear, which means that the material shows the elastic behavior; (ii) With the strain increases, the stress reaches yield stress, and then the curves show nonlinear, due to the fact that cracks occurs in the matrix and the material has permanent deformation. It should be mentioned that the yield stresses for different off-axis angles are quite diverse, on account of the speed of crack generation, and the off-axis will accumulate the speed. (iii) If the crack extends to the fiber bundles and leads to the failure of fibers, the stress reaches the third region, which means the damage in the material reaches saturation and the material loses its carrying capacity. It should be mentioned that the curves of 30° and 45° show obvious saturation region, and the curves of 0° and 90° are almost linear, dues to that the region of the damage saturation is short for 0° and 90° loading, and it will reach the failure stage rapidly. The reason for this phenomenon is that when the materials suffer 0° and 90° loading, loads are applied axially along with the fiber bundles, leading to the fast failure of fibers at the third region, while for 30° and 45° loading, the load is distributed across the fiber bundles.

The damage evolution process is demonstrated in Fig. 2(b), and the stress–strain curves for the CMCs after thermal shocks show similar behavior with the 0° original specimen, except that the elastic modulus decrease [31].

Besides, it can be recognized that the elastic modulus is inflected by the off-axis angle, 0° shows the maximum elastic modulus, and 45° shows the minimum ones. Since the locations of the cross-over for fiber bundles are different for 0° and 90° loadings (referring to Fig. 4), the bearing capacity of the materials in the 0° and 90° directions is different, causing the elastic modulus difference between 0° and 90° loading.

3. Establishment of the FE model

3.1. Woven fibers description

Since the braided structures of the woven composites possess the characteristic of periodicity, the repeat unit cell (RUC) is applied to obtain the effective properties of the woven materials, as well as to investigate the micro deformation during the loading.

To achieve the realism, the RUC should represent the real weave architecture and tow waviness of the woven composites. In the present work, the real paths of weft and warp tows were obtained by the SEM

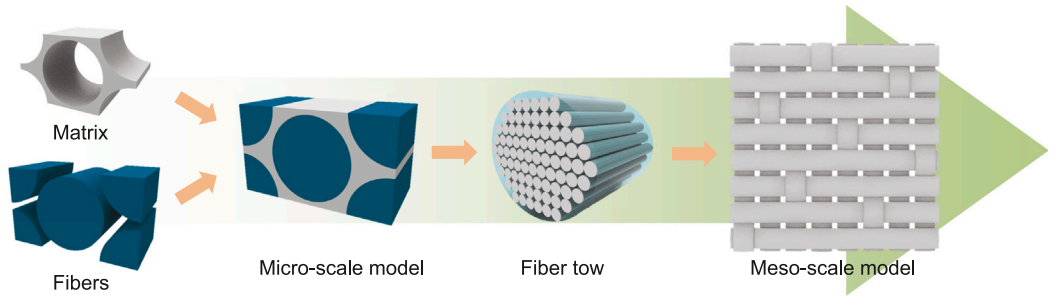

Fig. 5. The basic principle of the multiscale model, used to determine the property of fiber bundles, as fiber bundles contain fibers and matrix.

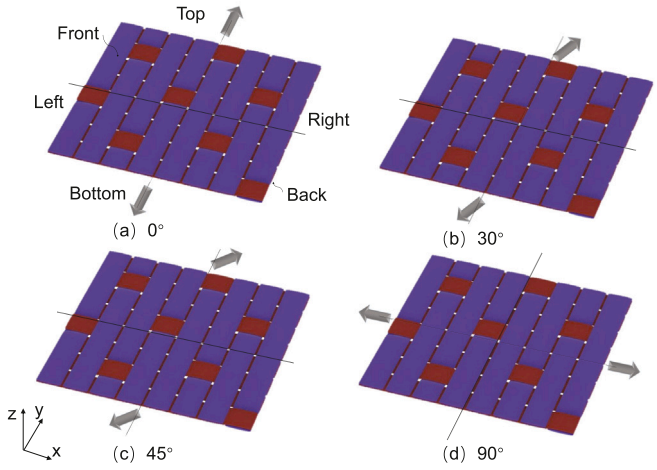

Fig. 6. Typical loading conditions used to investigate the effect of off-axis loading on mechanical response, ranging from (a) 0°, (b) 30°, (c) 45° and (d) 90°.

Table 1
The parameters to calculate the effective elastic modulus of matrix and fibers.

Parameter	η_0	a	E_m^0 (GPa)	E_f^0 (GPa)
Value	0.87	1.867	373	210

observation as depicted in Fig. 4(a). Besides, it is assumed that the tows are straight along the principal material directions, except for the cross-over region between tows. The cross-section of tows is expected to be elliptical, as for simplification.

The final weave architecture of the RUC is issued in Fig. 4(b), which contains eight weft tows and eight warp tows. In consideration of effective computation, each tow is modeled the same, and they are obtained by translating and rotating one tow, so that the cross-section and aspect ratios is identical to each other. The total tow volume in RUC are consistent of the total fiber volume of the entire material, which was achieved by adjusting the thickness of the matrix.

3.2. Preliminary determination of constituent properties

Direct specifying material constants of the matrix and fiber bundles using the manufacturer's data of the original matrix and fiber materials during the simulation is problematic. On the one hand, due to the porous nature of the matrix, it is unreasonable to regard the matrix in the ox/ox-CMCs as original matrix material, which will overrate the material properties. On the other hand, the fiber bundle, or tows, consists of fiber and porous matrix, so that the material properties of fiber bundles reflect the effective properties of fiber and porous matrix. In view of the consideration, a multiscale modeling method was applied to calibrate the material property of fiber and matrix, which is

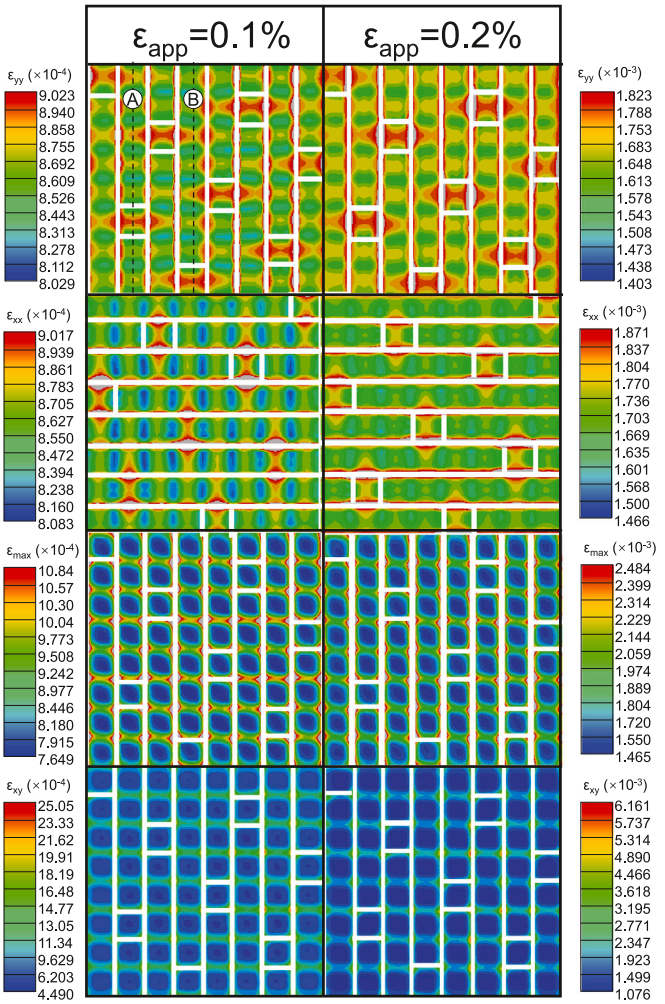

Fig. 7. Surface strains computed from different off-axis models. From the top-down, the figures represent the surface strains computed from 0°, 90°, 30°, 45° models. Overlaid white lines indicate tow boundaries. Two applied strain levels, 0.1% and 0.2%, were chosen to investigate the change of strain distribution when strain increases.

developed by the previous work [38]. The multiscale model contains the micro-scale model and the meso-scale model as shown in Fig. 5. The micro-scale model is established to obtain the effective mechanical properties of the fiber bundles. As the fiber bundles consist of fiber and matrix, an RUC of the fiber bundles (the micro-scale model) can be used to determine the effective elastic modulus and the Poisson's ratio of the total fiber bundles. Then, the meso-scale model is established considering the periodic braided structure of the fiber bundles, and the properties of the fiber bundles are obtained from the micro-scale

Table 2
The comparison between the computed elastic modulus of thermal-shocked CMCs and experiments.

Material	Original (GPa)	After 2nd thermal shocks (GPa)	After 8th thermal shocks (GPa)
Predictions	119.8	97.7	81.7
Experiments	120.5	98	82
errors	0.5%	0.3%	0.36%

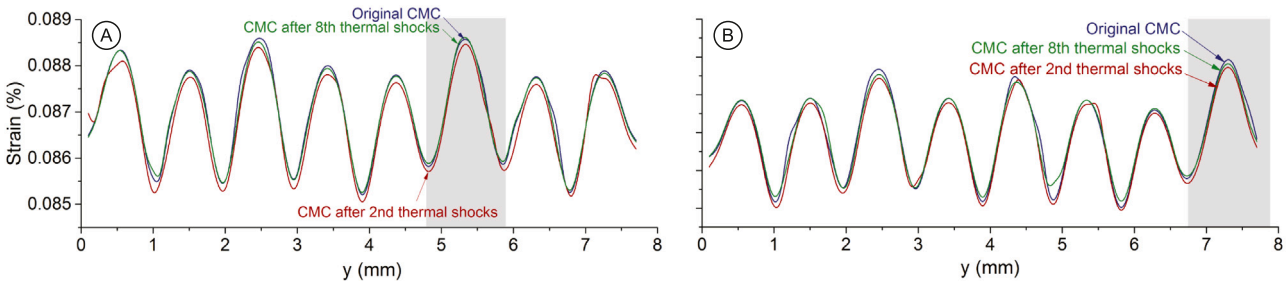

Fig. 8. The strains along two lines (line A and B in Fig. 7) under 0° loading with different cyclic thermal shocks.

model. The modeling details of the multiscale method are introduced as follows.

Firstly, to obtain the effective properties of porous matrix and fiber bundles, the authors have developed a micromechanics-based model considering the contribution of hierarchical pores [39]. The basic idea of the model is regarding the hierarchical pores as inclusions in materials but have zero stiffness, then the effective elastic modulus of matrix and fibers can be expressed as a function of hierarchical porosity:

$$E_f = \eta_0(1-\zeta_f-\zeta_m)^{a-1}E_f^0$$
$$E_m = (1-\zeta_f-\zeta_m)^{a-1}E_m^0$$

where η_0 represents the fiber orientation, and a is a material parameter. E_f^0 and E_m^0 are the elastic modulus of fiber and matrix without pores, respectively; ζ_f and ζ_m denote the porosity in the fiber and matrix. The parameters to calculate the effective elastic modulus of matrix and fibers are shown in Table 1. Besides, the porosities of the fiber and matrix are obtained by the mercury intrusion method, and verified by the micro-CT.

After obtained both the fiber and matrix property in the fiber bundles, a microscale finite element model will be established to determine the effective property of the fiber bundles, which will be regarded as input for the calculation of the mesoscale model.

The inputs of the meso-scale model contain the effective properties of the fiber bundles and the properties of the matrix. However, there are some initial manufacturing defects in the matrix, causing a decrease in the original properties of the matrix. Therefore, there will be a difference between the calculated properties of the ox/ox CMCs obtained by the meso-scale model and the experimental results, and an iterative procedure is necessary to reach higher fidelity after preliminary determining the constituent properties of the mesoscale model. The effective fiber bundle and matrix properties are used for simulation, and the results will be compared with the pertinent experimental results. If the computed results are quite different from the experimental results, then judiciously adjust the component parameters and conduct simulation, repeat the process until the results agree with the measurements. After some iterations, the mesoscale model can certainly reproduce the measurements accurately.

3.3. Loading and boundary conditions

Firstly, to investigate the effect of off-axis loading on mechanical response, typical off-axis loading conditions, ranging from 0°, 30°, 45° and 90°, was considered, as illustrated in Fig. 6. As the micro-scale model and the meso-scale model are based on the RUC, the periodic boundary conditions are applied to both the micro-scale and meso-scale models. The loading for the micro-scale model is the uniaxial tension loading along the spindle direction of the model. The loading to the meso-scale model is the off-axis tension loading along the 0°, 30°, 45° and 90° direction.

Secondly, the effect of thermomechanical loading was realized by changing the effective elastic modulus of fiber bundles and matrix, and the RUCs of CMCs after two and eight cyclic thermal shocks were established, the loading condition is loading in the 0° direction.

The mesh type of matrix and tows is 8-node linear brick, reduced integration, hourglass control (C3D8R). The total number of elements is 131,400, and the number of nodes is 191,379 for the meso-scale model. To verify the grid convergence, the grid was encrypted, and the total number of elements becomes 201,880. The corresponding nodes in the case of two kinds of grids were selected respectively, and the stress of the nodes at the same time was compared. The error of the two groups of simulation results is 0.1776%, which is less than 1%. Therefore, it can be considered that the mesh convergence is good and the simulation result is reliable.

4. Material response

4.1. Macroscopic response

To calibrate the proposed meso-scale model, the computed elastic modulus of thermal-shocked CMCs was compared with experiments, as demonstrated in Table 2. In general, the simulated results agree with the experimental results adequately. Therefore, the property of matrix and fiber bundles is confirmed without more effort.

Notably, the experimental results exhibit the nonlinear behavior with the strain increases, for two reasons: Firstly, the damage occurs in the matrix and fiber bundles of materials, leading to the degeneration of material property; Secondly, the tows will be geometrically softened, such as bent or straightened, during tensile loading in the real composites.

4.2. Strains distribution

To investigate the attribution of the inhomogeneous strain field on the material property of CMCs, the strain distributions with different off-axis angles are presented as full-field maps in Fig. 7; Two applied strain levels, 0.1% and 0.2%, were chosen to investigate the change of strain distribution when strain increases. From the top down, the figures in Fig. 7 represent the surface strains computed from 0°, 90°, 30°, 45° models.

From Fig. 7, as for the 0° axis loading, the location of the maximum strain is near the cross-overs of tows, to be more exact, the edges of the

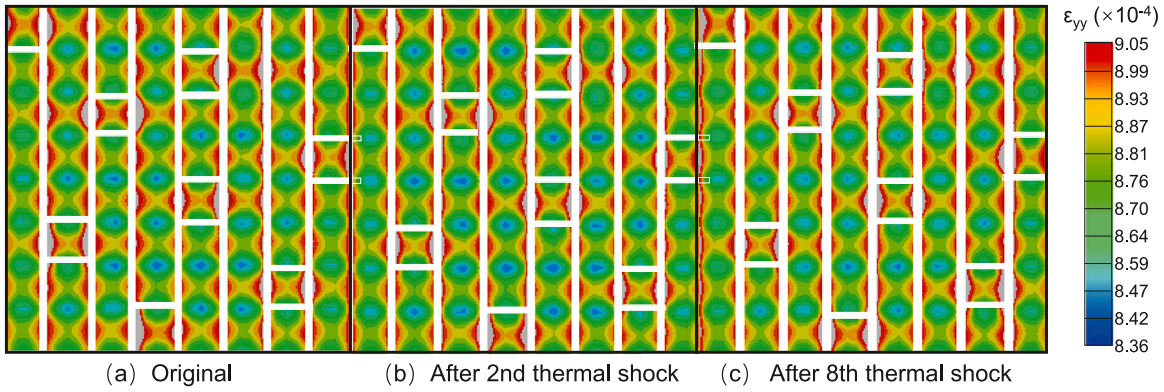

Fig. 9. Axial strain distribution with different cyclic thermal shocks under 0° loading. The phenomenon observed by thermal shocked CMC shows a similar tendency with the original CMC.

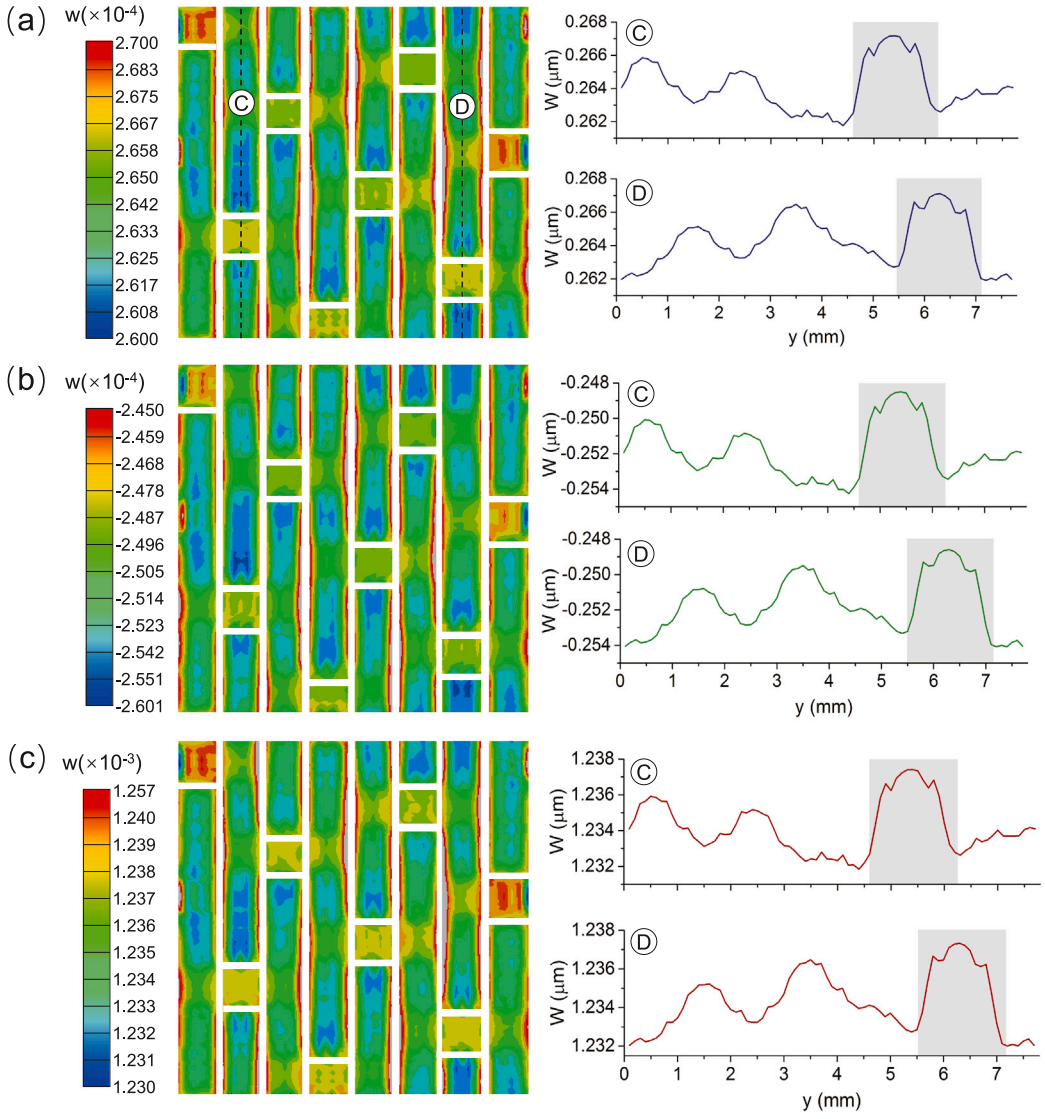

Fig. 10. Out-of-plane displacements under 0° tensile loading, at ε_{app}=0.2%, of (a) original CMC; (b) CMC after 2nd thermal shocks, and (c) CMC after 8th thermal shocks. The left figures are the total distribution of the RUC, the right figures are the displacement along two tows C and D.

cross-overs. The reason for this phenomenon is that the tows bend at the cross-over, leading to the stress concentration. Besides, the location near the tow cross-overs shows higher strains than the other areas of the tows, except for the edges, which is also due to the bending of the wavy sections, and the influence of beading will disappear with the distance increases. The strain distribution under 90° axis loading shows a similar

tendency, the maximum strain located in the edges of the cross-over. However, as for the 30° and 45° off-axis loading, the bending effects on the strain seems not obvious, due to the fact that the loading is not on axis, and the strain distribution for different tows shows a similar tendency. Because there are no tows along the loading direction, the strain distributions are demonstrated using the most obvious strain. In addition, with observation of the strain distribution for higher applied strain, it can be found that the phenomenon displayed at lower applied strain will be more distinct without change.

To quantify the axis strain distribution of one tow and verify the above analysis, two lines alone the axis of tows under 0° loading were chosen, which is exhibited in Fig. 7 as lines A and B. The strains along the lines were extracted, as demonstrated in Fig. 8. It can be seen that there are eight peaks along the line, and each peak indicates that there is a tow under the selected tow. The peak of the highest represents the location of the cross-over (seen gray regions), and there are tow second high peaks representing the location near the cross-over.

Meanwhile, to determine the damage and failure mechanism of the CMCs after thermal shocks, the effects of thermal shocks on the strain distribution were also investigated, and the axial strain with different cyclic thermal shocks under 0° loading are display in Fig. 9. The phenomenon observed by thermal shocked CMCs shows a similar tendency with the original CMCs, which has been described above. To further study the effects of thermal shocks, the axis strain distribution of one tow with different cyclic thermal shocks was exhibited in Fig. 8. The strains along the tows decrease with cyclic thermal shocks increase, which means that cyclic thermal shocks may affect the degree of constraint. This trend further exemplifies local tow bending and straightening as well as the effects of cyclic thermal shocks on the degree of constraint. Clearly, strain concentrations in cross-overs are an outward manifestation of the weave geometry and mechanical property mismatching.

Besides, the strain distributions can be used to predict the damage mechanism for CMCs after thermal shocks, as the damages initiation in the composites, such as the matrix cracks and delamination, are greatly influenced by the critical strain in the composites.

4.3. Out-of-plane displacement

After obtaining the strain distribution, the out-of-plane displacement for woven composites was also investigated. Fig. 10 shows the out-of-plane displacement w of original CMCs and thermal shocked CMCs under 0° tensile loading with the applied strain 0.2%, and the left figures are the total distribution of the RUC, the right figures are the displacement along two tows C and D. It can be seen from the left figures that, the out-of-plane displacement at the cross-over is higher than others, which is similar to the strain distribution, and the location near the cross-overs shows the lowest displacement due to the curvature of tows. Besides, the out-of-plane displacement is influenced by the curvature of tows, the location near the adjacent cross-over also shows the high displacement. This phenomenon can also be observed in the right figures. There are three peaks along the tow direction, the highest peak represents the location of the cross-over, and the other two show the locations near the adjacent cross-over.

The effects of off-axis loading and cyclic thermal shock condition on the strain concentration can be characterized by $k_\varepsilon = \varepsilon_{max}/\varepsilon_{app}$ (where ε_{max} is the maximum axial strain, ε_{app} is the applied strain). Fig. 11 illustrates the relationship between k and applied strain under different conditions. For all conditions, k_ε is essentially unchanged with the applied strain increases (independent of ε_{app}). However, k_ε increases with cyclic thermal shocks increase, varying from 2.18 to 2.22, and the off-axis angle also influences the value of k_ε.

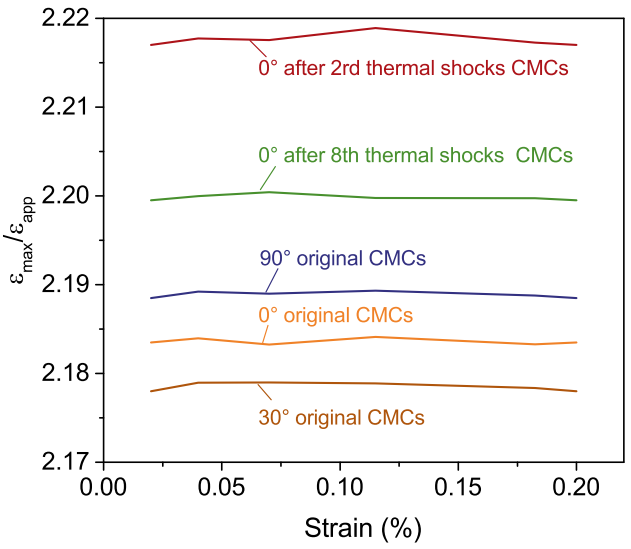

Fig. 11. Effects of off-axis load and cyclic thermal shock condition on the strain concentrations, characterized by $k_\varepsilon = \varepsilon_{max}/\varepsilon_{app}$ (with ε_{max} being the maximum axial strain).

4.4. Fiber stresses

The fiber stress distributions of original and thermal shocked CMCs under 0° tensile loading were demonstrated in Fig. 12. The maximum stress appears at the bending region of tows, and the adjacent region of tow cross-overs also shows fairly high stress. As for the influence of cyclic thermal shocks, with the cyclic thermal shocks increase, the stress decreases because the thermomechanical loading affects the mechanical property, and the elastic modulus degenerates. Besides, the average stress for the cross-sectional area of one tow (tow E in Fig. 12) along the axis direction with different cyclic thermal shocks was displayed in Fig. 13, and the error bars express the maximum and minimum of the stress in cross-sectional area. From the figure, the decrease in global stress can also be observed. The gray areas show the location of the cross-overs, and there is peak stress near the cross-overs.

The results of stress can give further information for the strain distribution. During 0° tensile loading, the transverse tows in cross-over areas are bent and the axial tows are straightened, leading to the stress increase. However, the maximum stress is obtained elsewhere: the edge of the axis tows near the cross-overs.

5. Discussion

In general, the strain and stress distribution have been acquired by the established meso-scale model, the effects of non-uniform stress and strain fields on the mechanical behavior can be investigated in the following:

(i) During the axis tensile loading, the axial tows were unaligned with the loading axis, leading to both tensile stress and bending stress within the tows. Therefore, the strain concentration appears at the edge of the cross-overs of tows.

(ii) As shown in Fig. 14(a), the axial surface tow was bent at the initial state. When suffering the axis loading, the axial surface tow tends to straighten, as illustrated by the dotted line. The straighten, in turn, causes the transverse tow to move, and the transverse tow on the cross-over tends to move up, leading to the out-of-plane displacement, the transverse tow near the cross-over moves sideways, resulting in the increase of axial strain.

(iii) Fig. 14(b) displays the observation of transverse tow, and it can be seen that the straighten of axial tow affects the bending of transverse

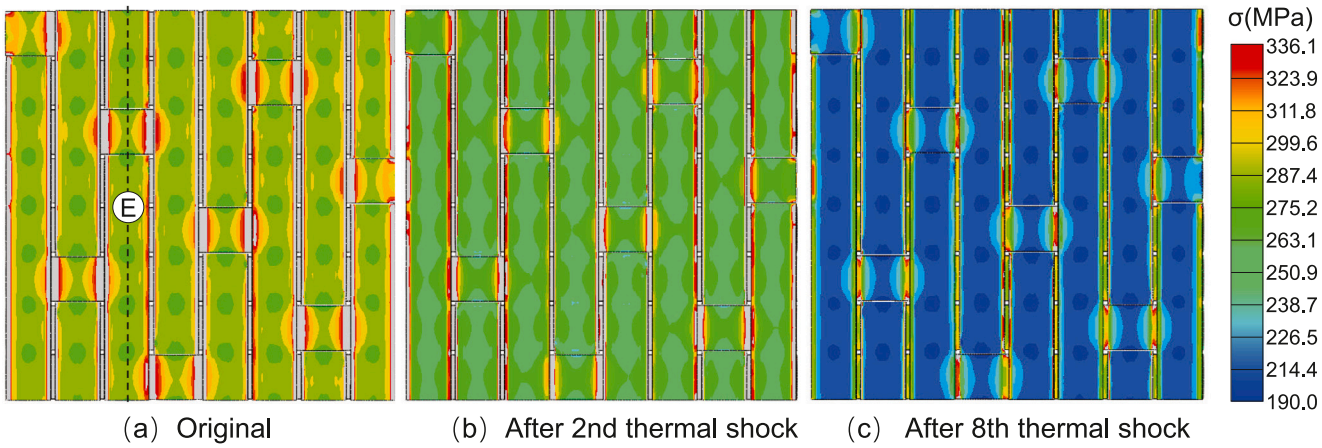

Fig. 12. Stress distributions of original and thermal shocked CMCs under 0° tensile loading, at ε_{app}=0.2%. (a) Original; (b) After 2nd thermal shocks; (c) After 8th thermal shocks. The maximum stress appears at the bending region of tows, and the adjacent region of tow cross-overs also show fairly high stress.

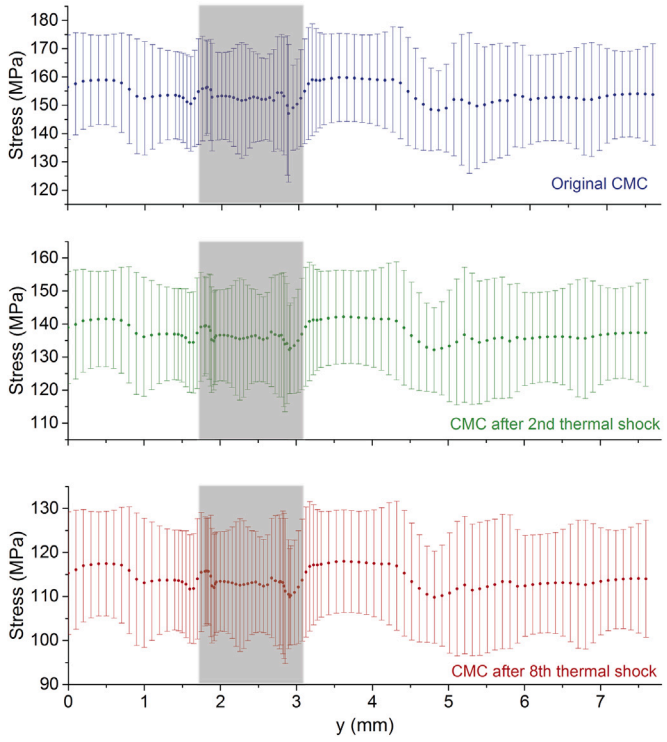

Fig. 13. Average stress for the cross-sectional area of one tow (tow E in Fig. 12) along the axis direction with different cyclic thermal shocks, and the error bars express the maximum and minimum of the stress in cross-sectional area.

tow, and leads to out-of-plane and transverse displacement, as well as high stress.

The thermomechanical loading can constrain the effects of non-uniform stress and strain fields discussed above, due to the degeneration of mechanical property. It should be noted that similar description can be found in Ref. [1], which can prove the discussion above.

The further conclusion can be obtained that, due to the stress concentration in the axial tows near the cross-overs, the strength for the woven composites may be inferior to that of laminate composites (the fibers in the composites are straight). Even though the progress of fiber fracture and coalescence leading to composite fracture depends on the length scale of stress height persistence and loading transfer characteristic between the fractured fiber and the surrounding material, the worst case scenario may be that the failure occurs at stresses that are inversely proportional to the rise in relative stresses. For example, if the peak stress rise to 20% and failure is assumed to occur at the local fiber stress reaches its inherent tow strength conservatively, the fracture stress will be reduced by $1 - 1/1.2 = 16.7\%$. A corresponding reduction in failure strain can be expected. Of course, the estimates ignore the complexity of tow failures as the fibers are not uniformly stressed: this problem remains unsolved.

The present data available for the woven composites obtained here and elsewhere seem to support the previous view, despite the difficulty to directly convert the predicted stress distribution into the failure strain of the composite material. In general, the ratios of these failure strains are consistent with the fiber stress heights calculated in this work.

The validity of the proposed meso-scale model needs more critical examination for woven composites. The comparisons between experiments and predictions under different loading conditions are required. Therefore, although the model and methods used in this study match the results of experiments, they may need some improvement to capture the behavior in a wider load range. For example, the nonlinearity of the mechanical property for woven CMCs under loading was not considered when modeling the RUC, which has been observed in experimental results. Despite these limitations of the present model, it is useful in providing insights into the origin and magnitude of stress/strain concentrations in woven composites under off-axis loading and thermomechanical loading.

6. Conclusions

The present work focuses on the tensile deformation response of 8HSW CMCs under non-uniform strain fields. The effects of weave architecture on stress and strain distributions of woven composites under off-axis loading and thermomechanical loading are investigated by establishing a meso-scale FE model. Although the scope of this work is limited to one type of weaving, it is expected that the modeling method can be useful in examining other types of weaving. The following conclusions are drawn for the study:

- A meso-scale FE model was established, and the real weave architecture was considered in the model. The weft and warp tow paths were determined by the SEM observation. Elements within the fiber tows were treated as being transversely isotropic, and the elements except the tows were ascribed to the property of matrix. Besides, the effects of porosity in the tows and matrix were taken into consideration in the model.
- The stress–strain response of the computed results was compared with experimental results. The results show that the method

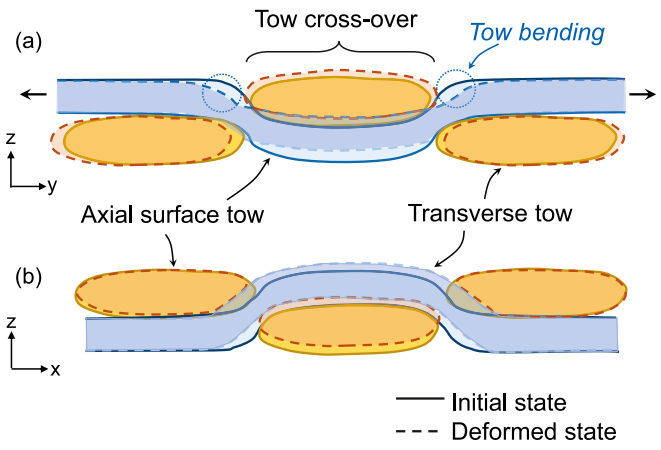

Fig. 14. Schematics showing: (a) when suffering the axis loading, the axial surface tow tends to straighten, as illustrated by the dotted line. The straighten, in turns, causes the transverse tow to move, resulting in the increase of axial strain; and (b) the observation of transverse tow, and it can be seen that the straighten of axial tow affects the bending of transverse tow, and leads to out-of-plane and transverse displacement, as well as the high stress [1].

can better match the tensile stress–strain curve at small applied strain, but underestimates the measured value at high applied strain. The difference between small and high strain is due to the degeneration of material property and the softening of the bending tows during experiments.

- As for the strain distribution, the maximum strain appears near the cross-overs of tows when CMCs under on-axis loading, due to the tows bending at the cross-over. Besides, the location near the tow cross-overs shows higher strains than the other areas of the tows. The bending effects on the strain seem not obvious under off-axis loading, and the strain distribution for different tows shows similar tendency.
- The stress distribution shows a similar tendency to strain, the maximum stress appears at the bending region of tows, and the adjacent region of tow cross-overs also shows fairly high stress. Besides, with the cyclic thermal shocks increase, the stress decreases due to the degeneration of the mechanical property.
- Due to the stress concentration in the axial tows near the cross-overs, the strength for the woven composites may be inferior to that of laminate composites, and the proposed model is useful in providing insights into the origin and magnitude of stress/strain concentrations in woven composites under off-axis loading and thermomechanical loading.

CRediT authorship contribution statement

Zheng-Mao Yang: Conceptualization, Methodology, Writing – review & editing, Writing – original draft, Visualization. **Jing-Yu Sun:** Investigation, Software. **Jun-Jie Yang:** Supervision. **Tian-Wei Liu:** Validation. **Hui Liu:** Data curation.

Declaration of competing interest

The authors declare that they have no known competing financial interests or personal relationships that could have appeared to influence the work reported in this paper.

Acknowledgments

The present work is supported by the National Natural Science Foundation of China (NSFC) (Grant No. 52105165), and the Strategic Priority Research Program of Chinese Academy of Sciences (Grant No. XDA17030100).

References

[1] Rossol MN, Rajan VP, Zok FW. Effects of weave architecture on mechanical response of 2D ceramic composites. Compos Part A-Appl Sci Manuf 2015;74(Supplement C):141–52.
[2] Sciti D, Galizia P, Reimer T, Schoberth A, Gutiérrez-Gonzalez CF, Silvestroni L, et al. Properties of large scale ultra-high temperature ceramic matrix composites made by filament winding and spark plasma sintering. Compos Part B: Eng 2021;216:108839.
[3] Mazars V, Caty O, Couegnat G, Bouterf A, Roux S, Denneulin S, et al. Damage investigation and modeling of 3D woven ceramic matrix composites from X-ray tomography in-situ tensile tests. Acta Mater 2017;140:130–9.
[4] Santhosh Unni, Ahmad Jalees, Ojard Greg, Smyth Imelda, Gowayed Yasser, Jefferson George. Effect of porosity on the nonlinear and time-dependent behavior of ceramic matrix composites. Compos Part B: Eng 2020;184:107658.
[5] Callaway E Benjamin, Zok Frank W. Tensile response of unidirectional ceramic minicomposites. J Mech Phys Solids 2020;138:103903.
[6] Appleby MP, Zhu Dongming, Morscher GN. Mechanical properties and real-time damage evaluations of environmental barrier coated SiC/SiC CMCs subjected to tensile loading under thermal gradients. Surface Coat Technol 2015;284:318–26.
[7] Flores Shane, Evans Anthony G, Zok Frank W, Genet Martin, Cox Brian, Marshall David, et al. Treating matrix nonlinearity in the binary model formulation for 3D ceramic composite structures. Compos Part A: Appl Sci Manuf 2010;41(2):222–9.
[8] Genet M, Marcin L, Baranger E, Cluzel C, Ladevže P, Mouret A. Computational prediction of the lifetime of self-healing CMC structures. Compos Part A: Appl Sci Manuf 2012;43(2):294–303.
[9] Del Puglia Paolo, Sheikh Mohammed A, Hayhurst David R. Classification and quantification of initial porosity in a CMC laminate. Compos Part A: Appl Sci Manuf 2004;35(2):223–30.
[10] Zhang Daxu, Liu Yu, Liu Hailong, Feng Yuqi, Guo Hongbao, Hong Zhiliang, et al. Characterisation of damage evolution in plain weave SiC/SiC composites using in situ X-ray micro-computed tomography. Compos Struct 2021;275:114447.
[11] Skinner Travis, Rai Ashwin, Chattopadhyay Aditi. Multiscale ceramic matrix composite thermomechanical damage model with fracture mechanics and internal state variables. Compos Struct 2020;236:111847.
[12] Kanouté P, Boso DP, Chaboche JL, Schrefler BA. Multiscale methods for composites: A review. Arch Comput Methods Eng 2009;16(1):31–75.
[13] Cox Brian N, Bale Hrishikesh A, Begley Matthew, Blacklock Matthew, Do Bao Chan, Fast Tony, et al. Stochastic virtual tests for high-temperature ceramic matrix composites. Annu Rev Mater Res 2014;44(44):479–529.
[14] Zhang Daxu, Hayhurst DR. Prediction of stress-strain and fracture behaviour of an 8-Harness satin weave ceramic matrix composite. Int J Solids Struct 2014;51(21–22):3762–75.
[15] Shojaei A, Li GQ, Fish J, Lan PJ. Multi-scale constitutive modeling of ceramic matrix composites by continuum damage mechanics. Int J Solids Struct 2014;51(23–24):4068–81.
[16] Leonetti Lorenzo, Greco Fabrizio, Trovalusci Patrizia, Luciano Raimondo, Masiani Renato. A multiscale damage analysis of periodic composites using a couple-stress/Cauchy multidomain model: Application to masonry structures. Compos Part B: Eng 2018;141:50–9.
[17] Colatosti Marco, Fantuzzi Nicholas, Trovalusci Patrizia. Time-history analysis of composite materials with rectangular microstructure under shear actions. Materials 2021;14(21):6439.
[18] Rajan VP, Zok FW. Effects of non-uniform strains on tensile fracture of fiber-reinforced ceramic composites. J Mech Phys Solids 2012;60(12):2003–18.
[19] Rajan Varun P, Zok Frank W. Remediation of a constitutive model for ceramic composite laminates. Compos Part A: Appl Sci Manuf 2013;52:80–8.
[20] Croom Brendan P, Xu Peng, Lahoda Edward J, Deck Christian P, Li Xiaodong. Quantifying the three-dimensional damage and stress redistribution mechanisms of braided SiC/SiC composites by in situ volumetric digital image correlation. Scripta Mater 2017;130:238–41.
[21] Hilmas Ashley M, Sevener Kathleen M, Halloran John W. Damage evolution in SiC/SiC unidirectional composites by X-ray tomography. J Am Ceram Soc 2020.
[22] Lu Zixing, Zhou Yuan, Yang Zhenyu, Liu Qiang. Multi-scale finite element analysis of 2.5D woven fabric composites under on-axis and off-axis tension. Comput Mater Sci 2013;79:485–94.
[23] Zhang Diantang, Liu Xiaodong, Gu Yuanhui, Sun Mengyao, Yu Song, Zhang Yifan, et al. Effects of off-axis angle on shear progressive damage of 3D woven composites with X-ray micro-computed tomography. Compos Part A: Appl Sci Manuf 2018;115:311–20.
[24] Yang Jishen, Yang Xiaoguang, Zhu Hanxing, Shi Duoqi, Chen Xindong, Qi Hongyu. The effect of off-axis angles on the mesoscale deformation response and failure behavior of an orthotropic textile carbon-epoxy composite. Compos Struct 2018;206:952–9.
[25] Kesba Mohamed Khodjet, Benkhedda A, Bedia EA Adda, Boukert B. Effect of high temperature on the stiffness properties of cracked composite laminates with different off-axis angles. Procedia Struct Integr 2020;28:864–72.

[26] Yang Chengpeng, Jia Fei, Wang Bo, Huang Tao, Jiao Guiqiong. Constitutive model and failure criterion for orthotropic ceramic matrix composites under macroscopic plane stress. J Am Ceram Soc 2021;104(2):1002–13.
[27] Kastritseas C, Smith PA, Yeomans JA. Thermal shock fracture in uni-directional fibre-reinforced ceramic-matrix composites. Compos Sci Technol 2005;65(11–12):1880–90.
[28] Kastritseas C, Smith PA, Yeomans JA. Thermal shock fracture in cross-ply fibre-reinforced ceramic-matrix composites. Philos Mag 2010;90(31–32):4209–26.
[29] Mei Hui, Cheng Laifei, Zhang Litong, Xu Yongdong. Effect of fiber architectures on thermal cycling damage of C/SiC composites in oxidizing atmosphere. Mater Sci Eng: A 2007;460–461:306–13.
[30] Han Geng, Guan Zhidong, Li Zengshan, Zhang Mi, Bian Tianya, Du Shanyi. Multi-scale modeling and damage analysis of composite with thermal residual stress. Appl Compos Mater 2015;22(3):289–305, identifier: 9407.
[31] Yang Zhengmao, Liu Hui. A continuum damage mechanics model for 2-D woven oxide/oxide ceramic matrix composites under cyclic thermal shocks. Ceram Int 2020;46(5):6029–37.
[32] Yang Zhengmao, Yuan Huang, Markert Bernd. Representation of micro-structural evolution and thermo-mechanical damage in thermal shocked oxide/oxide ceramic matrix composites. Int J Fatigue 2019;126:122–9.
[33] Zhang Xinghong, Wang Zhi, Hong Changqing, Hu Ping, Han Wenbo. Modification and validation of the thermal shock parameter for ceramic matrix composites under water quenching condition. Mater Des 2009;30(10):4552–6.
[34] Wu Shoujun, Cheng Laifei, Zhang Litong, Xu Yongdong. Thermal shock damage of a 3D-SiC/SiC composite. Adv Eng Mater 2010;7(11):1046–9.
[35] Kubit Andrzej, Trzepiecinski Tomasz, Kłonica Mariusz, Hebda Marek, Pytel Maciej. The influence of temperature gradient thermal shock cycles on the interlaminar shear strength of fibre metal laminate composite determined by the short beam test. Compos Part B: Eng 2019;176:107217.
[36] Ben Ramdane C, Julian-Jankowiak A, Valle R, Renollet Y, Parlier M, Martin E, et al. Microstructure and mechanical behaviour of a Nextel™ 610/alumina weak matrix composite subjected to tensile and compressive loadings. J Eur Ceram Soc 2017;37(8):2919–32.
[37] Yang Zhengmao, Liu Hui, Yuan Huang. Micro-porosity as damage indicator for characterizing cyclic thermal shock-induced anisotropic damage in oxide/oxide ceramic matrix composites. Eng Fract Mech 2019;220:106669.
[38] Yang Zhengmao, Yan Han. Multiscale modeling and failure analysis of an 8-harness satin woven composite. Compos Struct 2020;242:112186.
[39] Yang Zhengmao, Yan Han, Qian Guian, Ji Zhongdong. Influence of hierarchical porosity on the mechanical properties of porous woven composites under thermomechanical loading. Int J Solids Struct 2020;200–201:13–22.